

## Influence of multi-electron excitation on EXAFS spectroscopy of trivalent rare-earth ions and elucidation of change in hydration number through the series

ATSUYUKI OHTA,<sup>1,\*</sup> HIROYUKI KAGI,<sup>2</sup> HIROSHI TSUNO,<sup>3</sup> MASAHARU NOMURA,<sup>4</sup> AND IWAO KAWABE<sup>5</sup>

<sup>1</sup>Geological Survey of Japan, AIST, Tsukuba 305-8567, Japan

<sup>2</sup>Geochemical Laboratory, Graduate School of Science, The University of Tokyo, Tokyo 113-0033, Japan

<sup>3</sup>Faculty of Education and Human Sciences, Yokohama National University, Kanagawa, 240-8501, Japan

<sup>4</sup>Photon Factory, Institute of Materials Structure Science, KEK, Tsukuba 305-0801, Japan

<sup>5</sup>Department of Earth and Planetary Sciences, Graduate School of Environmental Studies, Nagoya University, Nagoya 464-8602, Japan

### ABSTRACT

We have made a detailed study of the extended X-ray absorption fine spectra (EXAFS) at the *K* edge of aqueous Y ion and at *L*<sub>3</sub> edges of aqueous lanthanide ions and thereby elucidated the systematic changes in their hydration structures. Anomalous peaks arising from double-electron excitation ( $2p, 4d \rightarrow 5d, 5d$ ) appear in the EXAFS signals of La<sup>3+</sup>-Tb<sup>3+</sup> between 5–7 Å<sup>-1</sup>. We established a removal process of double-electron excitation from EXAFS spectra. Using that process, we confirmed that the intensity and energy position of the extracted double-electron excitation are comparable to previously reported data. The presence of double-electron excitation engenders a smaller error than the errors estimated in the fitting process. Consequently, double-electron excitation does not seriously affect the determination of the structures of REE<sup>3+</sup> aquo ions in the first coordination sphere. Subsequent EXAFS analyses of hydrated REE<sup>3+</sup> ions suggest that the hydration numbers, the interatomic distances, and the Debye-Waller factors decrease from 9.7, 2.55 Å, and  $9.0 \times 10^{-3}$  Å<sup>2</sup> for La<sup>3+</sup> to 7.9, 2.31 Å, and  $5.7 \times 10^{-3}$  Å<sup>2</sup> for Lu<sup>3+</sup>. These parameters change as a sigmoid curve with increasing atomic number. The hydration structures of REE<sup>3+</sup> ions are inferred to change from the nonhydrated structure for La<sup>3+</sup>-Nd<sup>3+</sup> to the octahydrated structure for Tb<sup>3+</sup>-Lu<sup>3+</sup> through intermediate structures for Sm<sup>3+</sup>, Eu<sup>3+</sup>, and Gd<sup>3+</sup>. In addition, the hydration state of Y<sup>3+</sup> closely resembles that of Ho<sup>3+</sup> because the two have almost identical ionic radii.

**Keywords:** EXAFS, rare-earth elements, multi-electron excitation, hydration structure, structural change

### INTRODUCTION

Rare-earth element (REE) complexes are not isomorphous across the entire series because their ionic radii are influenced strongly by the lanthanide effect. For example, the hydration numbers of REE<sup>3+</sup> ions change from nine in the first coordination sphere for light REEs (La to Nd) to eight for heavy REEs (Tb-Lu), with intermediate ions (Sm to Gd) having eight or nine waters (Habenschuss and Spedding 1979a, 1979b, 1980). Change in the hydration structure causes anomalous behavior (“S-shape”) in thermodynamic and transport properties (Habenschuss and Spedding 1979a). However, little attention has been devoted to the effect of hydration change of REE aquo ions on thermodynamic properties in geochemistry. Kawabe (1999a, 1999b) and Kawabe et al. (1999) pointed out that the hydration change in the REE series strongly affects REE complexation by carbonate ions and REE partitioning between ferromanganese deposits and seawater. Moreover, Kawabe et al. (1999) and Ohta and Kawabe (2001) showed that the changes of REE coordination in solid phases (Fe oxyhydroxides and Mn dioxide) also affect REE partitioning coefficient patterns. Therefore, investigation

of REE coordination both in solid phases and liquid phases is an important study for geochemistry.

The REEs coprecipitated with or adsorbed on Fe-Mn oxides (or oxyhydroxides) both in nature and in the laboratory probably lack long-range order; their coordination states are unknown. Extended X-ray absorption fine structure (EXAFS) spectroscopy is applicable to structural analyses of such materials because it is highly selective to the central elements. In addition, the fluorescent mode is extremely sensitive to minor elements in samples. A disadvantage of the EXAFS method is its larger error for determination of coordination numbers because the coordination number strongly correlates to the Debye-Waller factor (Ohtaki and Radnai 1993). In addition, a small irregular feature caused by a multi-electron excitation is superimposed on the EXAFS oscillation of light REEs (Chaboy and Tyson 1994; Chaboy et al. 1994). Chaboy et al. (1994) and Solera et al. (1995) suggested that multi-electron excitation affects the determination of coordination number and interatomic distance. Different procedures to remove multi-electron excitation from EXAFS spectra have been introduced by researchers (e.g., Chaboy et al. 1994; Kodre et al. 1994; Solera et al. 1995; Allen et al. 2000). It is desirable that we establish an isolation process for the multi-electron excitation and systematically elucidate

\* E-mail: a.ohta@aist.go.jp

its influence on EXAFS data analysis. We have therefore determined the coordination structures of all REE (yttrium and lanthanides except Pm) ions in aqueous solutions using EXAFS spectroscopy. A simple EXAFS oscillation frequency of aqueous  $\text{REE}^{3+}$  ions facilitates identification of the multi-electron excitation (Solera et al. 1995). The hydration structures of REE ions have been obtained from several techniques (X-ray and neutron diffraction, EXAFS, Raman spectroscopy, molecular dynamics simulation, and so on) (e.g., Marcus 1988; Rizkalla and Choppin 1991; Ohtaki and Radnai 1993). These accumulated data help us to evaluate the reliability of EXAFS measurements. Kawabe et al. (1999) suggested that the coordination state of REE in Fe oxyhydroxide or Mn dioxide might be analogous to that of REE trihydroxides [ $\text{REE}(\text{OH})_3$ ] that have a hexagonal structure and consist of a nine-coordination sphere (Beall et al. 1977). Its coordination is a tricapped trigonal prism structure that is similar to the hydration structure of light  $\text{REE}^{3+}_{\text{aq}}$  (Rizkalla and Choppin 1991). Determination of the aqueous  $\text{REE}^{3+}$  structure is useful as a reference standard for REE in Fe-Mn materials.

## EXPERIMENTAL METHODS

### Samples and EXAFS spectroscopy

Commercially provided (Wako Pure Chemical Industries Ltd.) 1000 ppm solutions of  $\text{REE}^{3+}$  with 1 M  $\text{HNO}_3$  were prepared. The  $\text{REE}^{3+}$  aquo ions do not form inner sphere complexes with  $\text{NO}_3^-$  at concentrations lower than 1 M (Choppin et al. 1966; Choppin and Bertha 1973). For that reason, the results of EXAFS analyses of hydrated  $\text{REE}^{3+}$  ions in 1 M  $\text{HNO}_3$  solutions are comparable to the previously reported data for  $\text{REE}^{3+}$  hydration structures. Appendix 1 Tables 1 and 2<sup>1</sup> contain information about structural parameters of the hydration shell of  $\text{REE}^{3+}$  obtained by EXAFS (Yamaguchi et al. 1988; Solera et al. 1995; Bénazeth et al. 1998; Ishiguro et al. 1998; Ragnarsdottir et al. 1998; Allen et al. 2000; Lindqvist-Reis et al. 2000; Näslund et al. 2000; D'Angelo et al. 2001; Anderson et al. 2002; Mayanovic et al. 2002), X-ray diffraction (Russ et al. 1978; Habenschuss and Spedding 1979a, 1979b, 1980; Johansson and Wakita 1985; Johansson et al. 1985; Johansson and Yokoyama 1990), and neutron diffraction (Narten and Hahn 1982, 1983; Annis et al. 1985; Cossy et al. 1989; Helm and Merbach 1991; Yamaguchi et al. 1991).

The X-ray absorption fine structure (XAFS) spectra of  $\text{REE}^{3+}$  in nitrate solutions, which include X-ray absorption near-edge structure (XANES) and EXAFS regions were collected at the beamline BL12C of the Photon Factory at the High Energy Accelerator Research Organization (KEK-PF) in Tsukuba, Japan (Nomura and Koyama 1996). The KEK-PF storage ring was operated at 2.5 GeV with a 300–450 mA stored current. A Si(111) double-crystal monochromator produced a monochromatic X-ray beam with one crystal detuned to reduce harmonics. A bent cylindrical mirror focused the beam into an area smaller than  $1 \times 1$  mm (Nomura and Koyama 1996). The REE solutions were preserved in plastic bags and measured under atmospheric conditions at room temperature. The incident X-ray ( $I_0$ ) and transmitted X-ray ( $I_t$ ) intensities were monitored using ion chambers that were filled, respectively, with  $\text{N}_2$  gas and mixtures of  $\text{N}_2$  and Ar. The monochromator was calibrated at each Y-K edge (17040 eV) and Ln- $L_3$  edge (La, 5489 eV; Ce, 5727 eV; Pr, 5966 eV; Nd, 6214 eV; Sm, 6719 eV; Eu, 6982 eV; Gd, 7249 eV; Tb, 7518 eV; Dy, 7793 eV; Ho, 8072 eV; Er, 8360 eV; Tm, 8658 eV; Yb, 8947 eV; and Lu, 9246 eV) by recording the transmission signals from REE oxide (Y, La, Ce, Pr, Nd, Sm, Er, Tm, Yb, and Lu) or REE chloride hexahydrate (Eu, Gd, Tb, Dy, and Ho) powders. The Y-K edge and Ln- $L_3$  edge EXAFS spectra were recorded

using the fluorescence method of Y-K $\alpha$  and Ln-L $\alpha$ . Detuning was performed by reducing the incident flux to 70% for light REEs (La to Gd) and 80% for heavy REEs (Tb to Lu) and Y. The intensity of X-ray fluorescence ( $I_f$ ) was measured using a 19-element pure-Ge solid state detector (Nomura 1998). The energy region around the Y-K $\alpha$  or Ln-L $\alpha$  fluorescence was selected from elastic scattering by single-channel analyzers. The X-ray absorption [ $\mu(E)$ ] is expressed as  $\mu(E) = I_f/I_0$ . Multiple scans, typically 2–3, were carried out for each sample.

### EXAFS data analysis

Analyses of the XAFS spectra were performed using the computer program REX2000 (Rigaku Corp.). The measured XAFS spectra were averaged and then converted from energy to  $k$  space. The absorption threshold ( $E_0$ ) is defined as the inflection point of the absorption edge. The pre-edge background absorption [ $\mu_{\text{BK}}(E)$ ] is subtracted by extrapolating a linear polynomial fitted to the pre-edge absorbance through the post-edge region. The isolated atomic contribution to the absorption coefficient [ $\mu_0(E)$ ] is regarded as the smooth background in the EXAFS region fitted with a cubic spline curve. The resulting EXAFS signals are expressed as

$$\chi(k) = S_0^2 \sum_i \frac{N_i |F_i(k_i)|}{k_i R_i^2} \exp(-2k_i^2 \sigma_i^2) \exp\left(\frac{-2R_i}{\lambda_i}\right) \sin[2k_i R_i + \phi_i(k_i)] \quad (1)$$

where subscript  $i$  indicates the number of coordination spheres,  $\chi(k)$  is the EXAFS oscillation,  $S_0^2$  is the intrinsic loss factor,  $N_i$  is the coordination number,  $F_i(k_i)$  indicates the backscattering amplitude,  $k_i$  is the wavenumber,  $R_i$  is the interatomic distance,  $\sigma_i$  is the Debye-Waller factor,  $\lambda_i$  is the photoelectron mean-free path, and  $\phi_i(k_i)$  represents the phase shift.

A Fourier transform (FT) of the  $k^3$ -weighted EXAFS signals with a Hanning window function yielded a radial structure function (RSF). One major peak in the RSFs was isolated and back-transformed to  $k$  space. The determination of the coordination number ( $N_i$ ), the interatomic distance ( $R_i$ ), the threshold energy value ( $\Delta E_0$ ), and the Debye-Waller factor ( $\sigma_i$ ) for the isolated shell surrounding an absorber in an unknown material was produced using least-squares fitting of the Fourier-filtered  $k^3\chi(k)$  function. Theoretical backscattering amplitudes and phase shifts were calculated using FEFF 8.20 (Ankudinov et al. 2002). The REE ethyl sulfate enneahydrates [ $\text{REE}(\text{C}_2\text{H}_5\text{SO}_4)_9 \cdot 9\text{H}_2\text{O}$ ] were used as a model substance. All spectra were modeled using a single scattering REE-O path derived from REE ethyl sulfate enneahydrate because its structure is entirely isomorphous for all lanthanides (Gerkin and Reppart 1984). The coordination of hydrated  $\text{Y}^{3+}$  ion was determined using data for which Y is substituted for Ho in Ho ethyl sulfate enneahydrate. The amplitude reduction factor ( $S_0^2$ ) was fixed at 1.0 in all cases (Allen et al. 2000). The error was obtained from the square root of the diagonal elements in the covariance matrix that was estimated in the fitting calculation.

## RESULTS AND DISCUSSION

### The EXAFS oscillation

Figures 1a and 1b show that the EXAFS signals of aqueous  $\text{REE}^{3+}$  ions weighted by  $k^3$  are characterized by similar oscillating behavior, which reveals the existence of first shell local order around the REE site. A small feature at 5–7  $\text{\AA}^{-1}$ , which is indicated by an arrow in Figure 1a, is not expressed by a simple smooth sine curve. The feature is the multi-electron excitation and is assigned as the double-electron transition ( $2p, 4d \rightarrow 5d, 5d$ ) (Chaboy and Tyson 1994; Chaboy et al. 1994). Its intensity decreases and the position moves to the higher energy side as the atomic number  $Z$  increases; no significant structural change is visible above  $\text{Tb}^{3+}$  ion (see Figs. 1a and 1b). Solera et al. (1995) reported that the feature is recognized in aqueous  $\text{Dy}^{3+}$  ion. The feature comprises a doublet or broad peak, which might be related to relativistic splitting of the  $2p, 4d \rightarrow 5d, 5d$  transition (Chaboy and Tyson 1994; Solera et al. 1995). Another broad peak is superimposed on the EXAFS signal on the higher energy side, which is expressed by an area enclosed with a dotted line in Figure 1a. This structure becomes broader and shifts to the higher energy side with increasing  $Z$  number. Solera et al. (1995) described similar findings and pointed out that the feature might be related to chemical and/or structural effects.

<sup>1</sup> Deposit item AM-08-036, Appendix 1 Tables 1 and 2; Appendix 2 Tables 1, 2, and Figure 1. Deposit items are available two ways: For a paper copy contact the Business Office of the Mineralogical Society of America (see inside front cover of recent issue) for price information. For an electronic copy visit the MSA web site at <http://www.minsocam.org>, go to the American Mineralogist Contents, find the table of contents for the specific volume/issue wanted, and then click on the deposit link there.

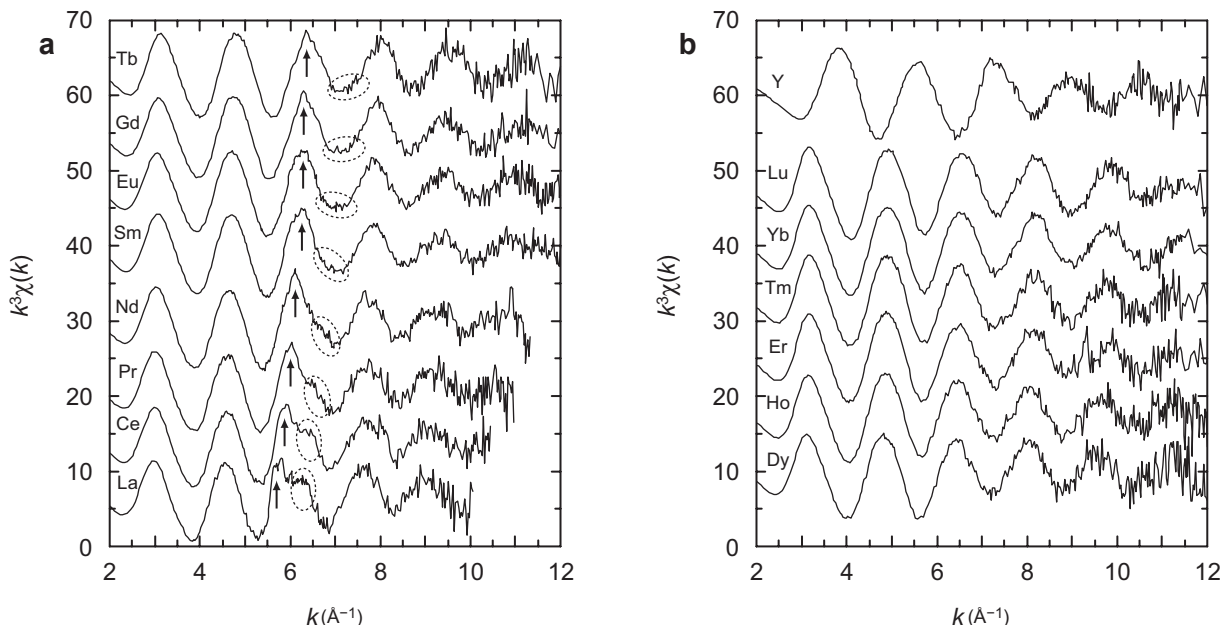


**FIGURE 1.** The  $k^3$ -weighted EXAFS signals of 1000-ppm REE<sup>3+</sup> ions in 1 M nitric acid solutions. (a)  $L_3$  EXAFS of La<sup>3+</sup>, Ce<sup>3+</sup>, Pr<sup>3+</sup>, Nd<sup>3+</sup>, Sm<sup>3+</sup>, Eu<sup>3+</sup>, Gd<sup>3+</sup>, and Tb<sup>3+</sup>. The arrow suggests the double-electron excitation ( $2p, 4d \rightarrow 5d, 5d$ ). The area enclosed with a dotted line shows an irregular peak aside from double-electron excitation. (b)  $L_3$  EXAFS of Dy<sup>3+</sup>, Ho<sup>3+</sup>, Er<sup>3+</sup>, Tm<sup>3+</sup>, Yb<sup>3+</sup>, and Lu<sup>3+</sup> and K EXAFS of Y<sup>3+</sup>. The spectra were shifted vertically for clarity.

## Elucidation of the multi-electron excitation

### Identification and removal of the multi-electron excitation.

The identification of multi-electron excitation is necessary to obtain structural information of light REE in materials accurately. Although various procedures have been introduced to extract multi-electron excitation from the EXAFS spectra (Chaboy and Tyson 1994; Chaboy et al. 1994; Kodre et al. 1994; Solera et al. 1995; Allen et al. 2000; Anderson et al. 2002), each method has its advantages and disadvantages. It is fundamentally desirable that the feature caused by the multi-electron excitation is removed not from the EXAFS oscillation [ $\chi(k)$ ], but from the absorption spectra [ $\mu(E)$ ] because X-ray absorption of the isolated atomic contribution [ $\mu_0(E)$ ], except the multi-electron excitation, should be recalculated from the data. We attempted to extract the multi-electron excitation from the underlying EXAFS spectra in a simple manner.

The EXAFS signal of aqueous ions, aside from the multi-electron excitations, is well represented by a single damped sine wave (Kodre et al. 1994). The EXAFS oscillation weighted with  $k^3$  can be fitted using the following equation that is modified from Filippini et al. (1988):

$$f_{\chi}(k) = (Ak^2 + B)\exp(-Ck^2)\sin(Dk^2 + Ek + F) + G + Hk \quad (2)$$

where A, B, C, D, E, F, G, and H are constants. Figure 2 shows an example of the identification of the multi-electron excitation: the EXAFS signal of aqueous La<sup>3+</sup> ion and the simple damped sine wave obtained as  $f_{\chi}(k)/k^3$ . Small anomalous peaks (a, b, c, and d in Fig. 2) are apparent in the region of 5–7 Å<sup>-1</sup>. The first two peaks (peaks a and b in Fig. 2) relate to the double-electron excitation ( $2p, 4d \rightarrow 5d, 5d$ ); the remainder (c and d in Fig. 2)

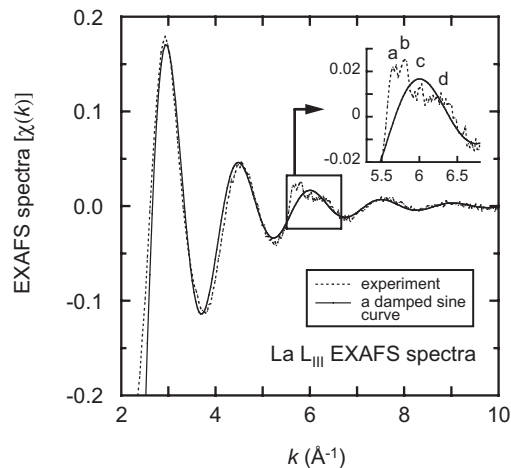


**FIGURE 2.** The EXAFS oscillation of La<sup>3+</sup><sub>(aq)</sub> (dotted line) and the best fit using a simple damped oscillation curve given by Equation 2 (solid line).

might be caused by some chemical and/or structural effect, as Solera et al. (1995) suggested. Kodre et al. (1994) subtracted the fitted curve from the EXAFS oscillation to isolate the multi-electron excitations for hydrated Cs<sup>+</sup>, Ba<sup>2+</sup>, and La<sup>3+</sup> ions. This procedure is straightforward, but it is disadvantageous in that the simple damped sine wave may not be well fitted to the EXAFS oscillation involving second-coordination and third-coordination spheres. It is also problematic that the extracted feature is indistinguishable from a residual oscillation or noise because the anomaly becomes inconspicuous with increasing Z number. Consequently, the simple damped sine wave fitted to the

EXAFS oscillation with Equation 2 is used as a guide to isolate the double-electron excitation.

Figures 3a and 3b show the removal process of the double-electron excitation from the absorption spectra of  $\text{La}^{3+}$  ion. Four anomalous peaks that appear in Figure 2 are visible in the region of 120–160 eV above  $E_0$  in Figure 3a. The guide curve is determined as  $[f_i(k)/k^3] \times \mu_0 + \mu_0 + \mu_{\text{BK}}$  when the EXAFS spectra are calculated as  $\chi(k) = (\mu - \mu_0 - \mu_{\text{BK}})/\mu_0$ . We assume that a smooth polynomial function (solid lines in Fig. 3a) represents the data in the absence of the double-electron excitation based on the guide curve (cross symbols in Fig. 3a). An electron transition is expressed by a Lorentzian function. Therefore, we extract the anomalous peaks from the absorption spectra with the smooth polynomial function (Fig. 3b) and then fit them with the following Lorentzian curve:

$$f_D(E) = \frac{A}{1 + 4 \frac{(E - E_D)^2}{W^2}} \quad (3)$$

where  $E_D$  denotes the energy of double-electron transition ( $2p, 4d \rightarrow 5d, 5d$ ),  $W$  is the width for the transition, and  $A$  is the constant

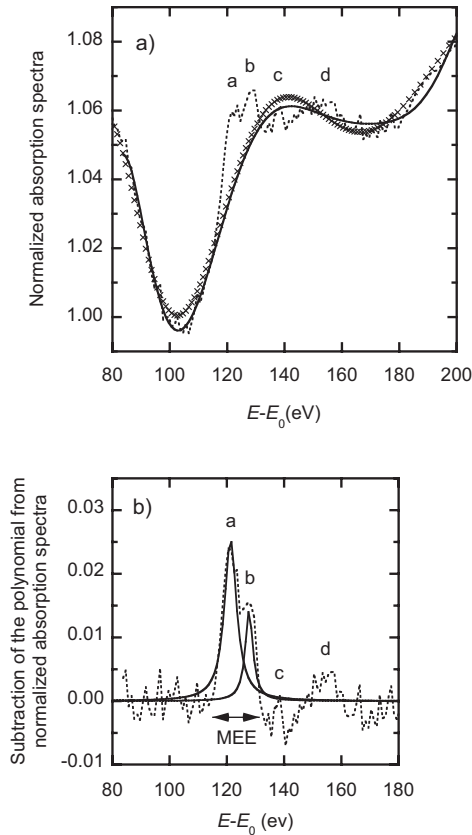


**FIGURE 3.** The removal process of the double-electron excitation structures found in  $L_3$ -absorption spectra of  $\text{La}_{\text{aq}}^{3+}$ . (a) The absorption spectrum (dotted line) is fitted by a polynomial function (solid line) based on the guide curve (cross symbols) obtained from the simple damped sine wave (see text). (b) Features arising from double-electron excitation extracted using the polynomial (dotted line) are fitted by two Lorentzian curves (solid lines).

expressing the intensity. The respective features of the double-electron excitations of  $\text{La}^{3+}$ ,  $\text{Ce}^{3+}$ ,  $\text{Pr}^{3+}$ ,  $\text{Nd}^{3+}$ ,  $\text{Sm}^{3+}$ , and  $\text{Eu}^{3+}$  ions are duplicated peaks, but those of  $\text{Gd}^{3+}$  and  $\text{Tb}^{3+}$  ions are small and broad peaks. Therefore, anomalous features of the former six ions were fitted by two Lorentzian functions (see  $\text{La}^{3+}$  in Fig. 3b); those of the remaining ions were fitted using a Lorentzian function. The final results show that we have subtracted the obtained Lorentzian functions that depict the double-electron excitation from the absorption spectra, and have completed the EXAFS analysis.

**Validity of the removal process of multi-electron (double-electron) excitation.** We compared the intensity and position of the double-electron excitation of  $\text{REE}^{3+}$  ions with experimental and theoretical values to confirm the reliability of our removal process (Chaboy and Tyson 1994; Chaboy et al. 1994; Solera et al. 1995). The intensity of the double-electron excitation is expressed as the value relative to that of the single-electron excitation at the  $L_3$  edge. The experimental  $L_3$  edge region was deconvoluted using Lorentzian and arctangent functions as the following equation:

$$f_s(E) = \frac{A}{1 + 4 \frac{(E - E_S)^2}{W^2}} + B \arctan[E - (E_S + \delta)] + C + DE \quad (4)$$

where  $E_S$  is the energy of the single-electron excitation ( $2p \rightarrow 5d$ ),  $W$  is the width for the main transition;  $\delta$  is the phase shift, and  $A$ ,  $B$ ,  $C$ , and  $D$  are constants. Figure 4 shows the deconvolution process of the  $\text{La}^{3+}$ - $L_3$  absorption edge region. The Lorentzian peak area gives the transition cross section ( $\sigma$ ), which expresses the intensity of the transition (Chaboy et al. 1994; Solera et al. 1995). The ratio of cross section strength between double-electron and single-electron excitations ( $\sigma_D/\sigma_S$ ) is estimated as the area ratio of the Lorentzian peaks used for the deconvolution model of each excitation (Figs. 3b and 4). The relative position of the double-electron excitation to the single-electron excitation ( $\Delta E$ ) is calculated as the difference between the absorption edge ( $E_0$ ) and the central axis or peak top of the double-electron excitation.

Table 1 shows the experimental and theoretical  $\sigma_D/\sigma_S$  ratios and  $\Delta E$  values of  $\text{REE}^{3+}$  ions. The estimated  $\sigma_D/\sigma_S$  ratios are very consistent with those determined by Solera et al. (1995), but they are only half of the theoretical values. The decrease of experimental  $\sigma_D/\sigma_S$  ratios with the atomic number is more rapid than for the theoretical values, as Solera et al. (1995) suggested. The  $\Delta E$  values estimated in the present study are also consistent with those obtained by Solera et al. (1995). Neither the experimental  $\Delta E$  values obtained in the present study nor those by Solera et al. (1995) agree completely with the theoretical values. However, the systematic trend of increasing experimental  $\Delta E$  with increasing atomic number concurs with the theoretical values to some degree. In conclusion, our removal process for the double-electron excitation features is reasonable. The deviation of experimental  $\sigma_D/\sigma_S$  ratios and  $\Delta E$  values from the theoretical values is possibly attributable to the theoretical model: Chaboy and Tyson (1994) used the atomic orbitals of REE for calculations. They suggested that the theory must be generalized to the cluster case by replacing valence orbitals with molecular orbitals in a rigorous manner.

**TABLE 1.** Intensities and excitation energies of double-electron excitations for the lanthanide series

	$\sigma_D/\sigma_S$ (%) <sup>*</sup>			$\Delta E$ (eV) <sup>†</sup>		
	This study	Solera et al. (1995)	Theoretical value <sup>‡</sup>	This study	Solera et al. (1995)	Theoretical value <sup>‡</sup>
La	1.3 ± 0.2	1.2 ± 0.2	2.16	123 ± <1	125 ± 5	123
Ce	1.1 ± 0.2	1.1 ± 0.2 <sup>§</sup>	1.66	128 ± <1	127 ± 5 <sup>§</sup>	122
Pr	0.8 ± 0.2	0.74 ± 0.2 <sup>§</sup>	1.4	134 ± 1	129 ± 5 <sup>§</sup>	128
Nd	0.6 ± 0.1	0.7 ± 0.2	1.2	141 ± <1	135 ± 5	134
Sm	0.6 ± 0.1		0.91	150 ± 1		146
Eu	0.5 ± 0.4	0.5 ± 0.2	0.802	151 ± 1	156 ± 5	152
Gd	0.3 ± 0.1		0.838	152 ± <1		166
Tb	0.2 ± 0.1		0.63	154 ± <1		164
Dy		0.2 ± 0.2	0.567		162 ± 5	170
Ho			0.51			177
Er			0.46			183
Tm			0.42			189
Yb			0.38			196
Lu			0.38			210

<sup>\*</sup> The relative ratio of the cross section strength of double-electron excitation to that of single-electron excitation.

<sup>†</sup> The energy difference between double-electron excitation and  $E_0$ .

<sup>‡</sup> Data were cited from Chaboy and Tyson (1994) and Chaboy et al. (1994).

<sup>§</sup> The  $\sigma_D/\sigma_S$  and  $\Delta E$  data of Ce and Pr in Solera et al. (1995) were replaced at the authors' discretion.

|| Digitized values of Chaboy and Tyson (1994).

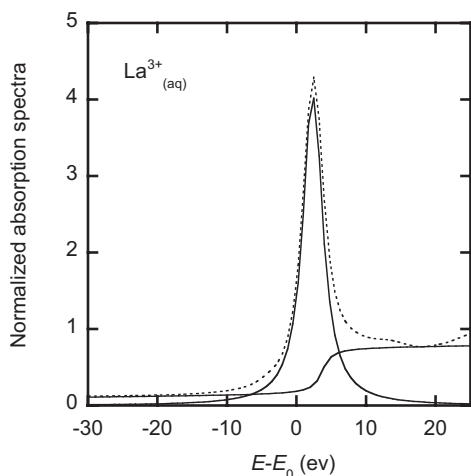


**FIGURE 4.** The deconvolution procedure of  $L_3$ -absorption spectra of  $\text{La}^{3+}_{(\text{aq})}$ . The main transition of  $2p \rightarrow 5d$  (dotted line) is fitted by a Lorentzian function and a continuum spectrum (solid lines), which are given by Equation 4.

### Determination of local structure of $\text{REE}^{3+}_{(\text{aq})}$ and radial structure functions

Figure 5 shows the RSFs for all  $\text{REE}^{3+}$  ions for which the double-electron excitation was corrected for light  $\text{REE}^{3+}$  ions. The results of the curve-fits are also shown in Figure 5 and Table 2. Their RSFs have one major peak at 1.8–2.0 Å (the phase shift is uncorrected) and some small ripples beside the main peak. The ripples observed at values less than 1.0 Å (the phase shift is uncorrected) are low-frequency noises arising from imperfect subtraction of the smooth background absorption; small peaks beside the main peak are side lobes generated in the FT (Yamaguchi et al. 1988).

First, we specifically examine the effect of double-electron excitation on EXAFS analysis. Chaboy et al. (1994) analyzed EXAFS data of crystalline  $\text{CeF}_2$  and  $\text{CeF}_2\text{H}_{3.75}$  by performing FT in the  $k$ -range of 2.5–10.4 Å<sup>-1</sup>. They reported that the influence of the double-electron excitation implies a correction of about 10% on the coordination number with no modification of the

interatomic distance. Solera et al. (1995) performed FT in the  $k$ -range of 2.5–9.0 Å<sup>-1</sup> on EXAFS spectra of aqueous  $\text{REE}^{3+}$  ions. They reported that the interatomic distance becomes 0.02 Å smaller for  $\text{La}^{3+}$ ,  $\text{Ce}^{3+}$ , and  $\text{Pr}^{3+}$  ions, 0.01 Å smaller for  $\text{Nd}^{3+}$  ion, and that it is unchanged for  $\text{Eu}^{3+}$  ion after removing the double-electron excitation. However, the parameters determined in this study are almost identical to the original data, within respective errors. Table 2 shows that the hydration numbers become 0.2 larger for  $\text{La}^{3+}$  and 0.2–0.5 smaller for  $\text{Ce}^{3+}$ – $\text{Tb}^{3+}$ , the interatomic distances become 0.002–0.005 Å shorter for  $\text{La}^{3+}$ – $\text{Pr}^{3+}$  and change slightly for  $\text{Nd}^{3+}$ – $\text{Tb}^{3+}$ ; the shift of  $E_0$  becomes 0.1–0.6 eV higher, and the Debye-Waller factors become  $0.1$ – $0.7 \times 10^{-3}$  Å<sup>2</sup> larger after correcting the double-electron excitation. It is concluded, therefore, that double-electron excitation does not seriously affect the determination of the structures of  $\text{REE}^{3+}$  aquo ions in the first coordination sphere.

In contrast to  $\text{REE}^{3+}$  aquo ion, the interatomic distance for  $\text{La}^{3+}$  adsorbed on Fe hydroxides and Mn dioxides becomes 0.01–0.03 Å shorter and hydration number becomes 0.3–1.0 smaller after the correction for multi-electron excitation (unpublished data). (We will discuss the importance of the correction for a multi-electron excitation in these systems in another paper.) Therefore, the removal process of the multi-electron excitation, as established in this study, is effective in the precise determination of the coordination structures of light REEs complexes, especially for La.

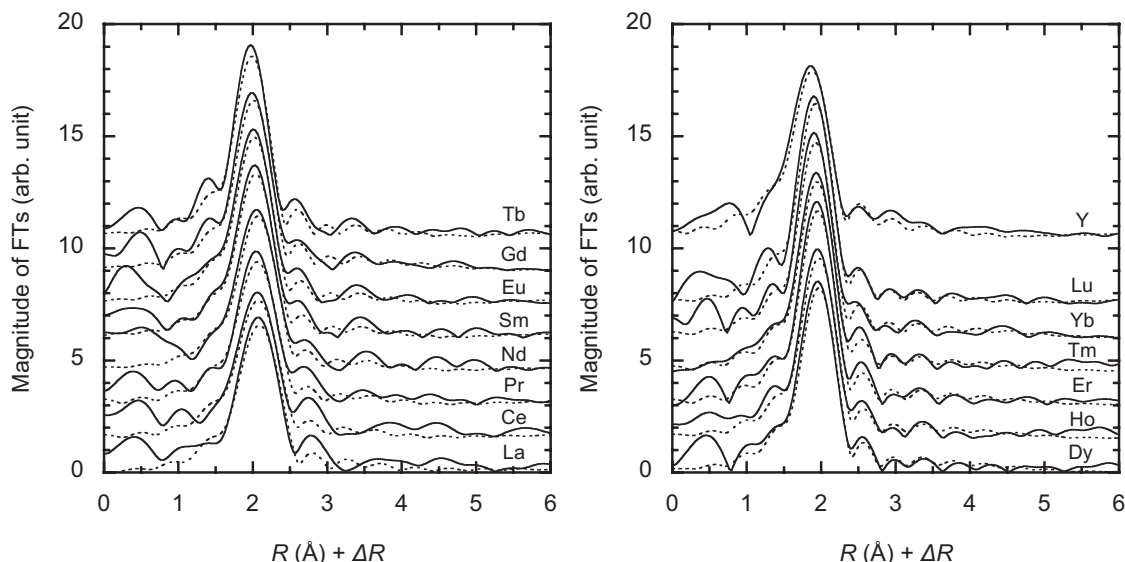
### Precision and accuracy of determined local structure of $\text{REE}^{3+}$ ions

The precision of determined structural parameters of  $\text{REE}^{3+}$  ions was examined using EXAFS analyses of four measurements of  $\text{Yb}^{3+}_{(\text{aq})}$ . The calculated mean and e.s.d. for each parameter are as follows: 7.66(5) for the hydration number, 2.319(3) Å for the interatomic distance, –2.0(2) eV for  $\Delta E_0$ , and  $5.9(1) \times 10^{-3}$  Å<sup>2</sup> for the Debye-Waller factor. These errors, calculated from repeated measurements, are smaller than the errors estimated in the fitting process (Table 2). As long as the fitting procedure and parameters such as background extraction method and model compounds used in the FEFF calculation are common among REE samples, the obtained parameters can yield high precision.

**TABLE 2.** EXAFS curve-fitting summary of  $\text{REE}^{3+}_{(\text{aq})}$  in 1  $N$   $\text{HNO}_3$  for hydration numbers ( $N$ ), interatomic distances ( $R$ ), the shift of threshold energy ( $\Delta E_0$ ), and the Debye-Waller factors ( $\sigma^2$ )

Element	Run no.	$N$		$R$ (Å)		$\Delta E_0$ (eV)		$\sigma^2$ ( $\times 10^{-3}$ Å <sup>2</sup> )		$k$ range (Å <sup>-1</sup> )
Y	1	7.5 ± 0.6		2.362 ± 0.005		-11.1 ± 0.8		6.4 ± 1.4		3.35–11.55
La	1	9.4 ± 1.0	9.6 ± 0.8*	2.560 ± 0.007	2.555 ± 0.007*	-2.6 ± 0.8	-2.0 ± 0.7*	8.5 ± 2.0	9.2 ± 2.1*	2.60–10.00
	2	9.6 ± 0.7	9.8 ± 0.7*	2.552 ± 0.007	2.547 ± 0.007*	-2.4 ± 0.7	-1.9 ± 0.7*	8.5 ± 2.0	8.8 ± 2.1*	2.60–10.00
Ce	1	9.5 ± 0.7	9.4 ± 0.8*	2.520 ± 0.007	2.517 ± 0.007*	-2.7 ± 0.8	-2.2 ± 0.8*	9.2 ± 2.1	9.4 ± 2.1*	2.65–10.50
	Pr	1	9.7 ± 0.6	9.3 ± 0.7*	2.503 ± 0.007	2.501 ± 0.007*	-2.8 ± 0.8	-2.5 ± 0.8*	8.8 ± 2.1	9.0 ± 1.9*
Nd	2	10.5 ± 0.7	10.2 ± 0.7*	2.505 ± 0.007	2.502 ± 0.007*	-2.4 ± 0.8	-2.3 ± 0.8*	9.8 ± 2.0	9.8 ± 2.0*	2.65–10.70
	1	9.9 ± 0.7	9.4 ± 0.7*	2.488 ± 0.006	2.487 ± 0.006*	-2.0 ± 0.7	-1.8 ± 0.7*	8.3 ± 1.6	8.5 ± 1.7*	2.65–11.00
Sm	2	10.2 ± 0.7	9.9 ± 0.7*	2.490 ± 0.006	2.491 ± 0.007*	-1.7 ± 0.7	-1.5 ± 0.8*	8.6 ± 1.7	9.0 ± 1.7*	2.65–11.00
	1	9.4 ± 0.6	9.0 ± 0.6*	2.442 ± 0.006	2.443 ± 0.006*	-2.7 ± 0.8	-2.7 ± 0.8*	7.9 ± 1.6	8.1 ± 1.6*	2.75–11.30
Eu	2	9.5 ± 0.6	9.2 ± 0.6*	2.448 ± 0.006	2.449 ± 0.006*	-1.5 ± 0.7	-1.4 ± 0.8*	7.9 ± 1.6	8.1 ± 1.6*	2.75–11.30
	1	8.5 ± 0.6	8.3 ± 0.6*	2.430 ± 0.006	2.431 ± 0.006*	-1.9 ± 0.7	-1.9 ± 0.8*	6.7 ± 1.5	6.9 ± 1.5*	2.75–11.30
Gd	2	9.1 ± 0.6	8.8 ± 0.6*	2.430 ± 0.006	2.431 ± 0.006*	-2.3 ± 0.7	-2.2 ± 0.8*	7.4 ± 1.5	7.4 ± 1.5*	2.75–11.30
	1	8.1 ± 0.5	7.9 ± 0.5*	2.408 ± 0.005	2.408 ± 0.005*	-2.1 ± 0.7	-2.1 ± 0.7*	6.4 ± 1.4	6.6 ± 1.5*	2.75–11.50
Tb	1	8.0 ± 0.5	7.8 ± 0.5*	2.383 ± 0.005	2.383 ± 0.005*	-2.0 ± 0.7	-1.9 ± 0.7*	5.9 ± 1.2	5.9 ± 1.4*	2.75–11.50
Dy	1	8.0 ± 0.5		2.370 ± 0.005		-2.2 ± 0.6		6.2 ± 1.3		2.75–11.50
	2	8.0 ± 0.5		2.379 ± 0.005		-1.2 ± 0.6		6.4 ± 1.4		2.75–11.50
Ho	1	7.9 ± 0.5		2.360 ± 0.005		-1.2 ± 0.6		6.4 ± 1.3		2.80–11.50
	Er	1	8.5 ± 0.5		2.341 ± 0.005		-1.5 ± 0.6		7.4 ± 1.4	
Tm	2	7.7 ± 0.4		2.343 ± 0.004		-1.4 ± 0.6		5.6 ± 1.2		2.80–11.50
	1	7.9 ± 0.5		2.332 ± 0.005		-1.1 ± 0.6		6.2 ± 1.3		2.80–11.50
Yb	2	7.9 ± 0.5		2.338 ± 0.004		-0.8 ± 0.6		5.9 ± 1.2		2.80–11.50
	1	7.6 ± 0.4		2.315 ± 0.004		-2.2 ± 0.6		5.8 ± 1.2		2.80–11.50
Lu	2	7.7 ± 0.4		2.320 ± 0.004		-1.8 ± 0.6		5.9 ± 1.2		2.80–11.50
	3	7.7 ± 0.5		2.319 ± 0.004		-1.8 ± 0.6		5.9 ± 1.2		2.80–11.50
Lu	4	7.7 ± 0.4		2.321 ± 0.004		-2.0 ± 0.6		5.8 ± 1.2		2.80–11.50
	1	7.9 ± 0.4		2.310 ± 0.004		-2.4 ± 0.6		5.9 ± 1.2		2.80–11.55
2	7.8 ± 0.4		2.315 ± 0.004		-2.1 ± 0.6		5.5 ± 1.2		2.80–11.55	

\*The EXAFS signals were corrected for double-electron excitation.

**FIGURE 5.** The RSFs of all hydrated  $\text{REE}^{3+}$  ions and the fitting results (dotted lines): (a) RSFs of  $\text{La}^{3+}$ ,  $\text{Ce}^{3+}$ ,  $\text{Pr}^{3+}$ ,  $\text{Nd}^{3+}$ ,  $\text{Sm}^{3+}$ ,  $\text{Eu}^{3+}$ ,  $\text{Gd}^{3+}$ , and  $\text{Tb}^{3+}$  ions; (b) RSFs of  $\text{Dy}^{3+}$ ,  $\text{Ho}^{3+}$ ,  $\text{Er}^{3+}$ ,  $\text{Tm}^{3+}$ ,  $\text{Yb}^{3+}$ ,  $\text{Lu}^{3+}$ , and  $\text{Y}^{3+}$ . The double-electron excitation has been corrected. The spectra are shifted vertically for clarity.

Next, we have confirmed the accuracy of EXAFS analyses through comparison of predicted structural parameters of aqueous  $\text{REE}^{3+}$  ions with reported values. Table 3 presents the determined structural parameters in this study, along with the means of the previous data obtained using the X-ray diffraction (XD) and neutron diffraction (ND), and EXAFS methods. Marcus (1988) suggested that the ion-water internuclear distances obtained by EXAFS are generally and systematically 1–2% shorter than those obtained from XD or ND. Table 3 shows

that the  $\text{REE-OH}_2$  distances obtained previously by EXAFS are systematically about 0.005–0.030 Å shorter than those by XD and are roughly consistent with those by ND. The deviation of the  $\text{REE-OH}_2$  distances determined using the EXAFS method from those by the XD and ND methods is not so serious as the result from Marcus (1988). However, caution is in order when comparing the  $\text{REE-OH}_2$  distances obtained by EXAFS to those by XD because the systematic differences of 0.005–0.030 Å are larger than the error of EXAFS analysis.

**TABLE 3.** Comparison of the hydration numbers ( $N$ ), the interatomic distances ( $R$ ), and the Debye-Waller factors ( $\sigma^2$ ) of  $\text{REE}^{3+}_{(\text{aq})}$ , as determined using the EXAFS, X-ray diffraction, and neutron diffraction methods (XD and ND)

	$N$				$R$ (Å)				$\sigma^2$ ( $\times 10^{-3}$ Å <sup>2</sup> )	
	This study	EXAFS	XD	ND	This study	EXAFS	XD	ND	This study	EXAFS
Y	7.5	9.0	8.0		2.362	2.361	2.366		6.4	6.0
La	9.7	8.9	8.6		2.551	2.557	2.575		9.0	8.5
Ce	9.4	9.2			2.517	2.529			9.4	7.9
Pr	9.7	9.0	9.2	10	2.502	2.512	2.539	2.48	9.0	8.0
Nd	9.7	9.3	8.9	9.0	2.489	2.497	2.513	2.489	8.7	8.6
Sm	9.1	9.2	8.4	8.5	2.446	2.453	2.465	2.467	8.1	6.2
Eu	8.5	8.7	8.3		2.431	2.435	2.45		7.1	7.4
Gd	7.9	7.8	9.9		2.408	2.413	2.40		6.6	6.1
Tb	7.8	7.8	8.1	9.0	2.383	2.390	2.403	2.39	5.9	5.1
Dy	8.0	8.1	7.9	8.1	2.375	2.371	2.396	2.386	6.3	6.0
Ho	7.9	8.0			2.360	2.359			6.4	5.5
Er	8.1	7.9	8.0		2.342	2.345	2.36		6.5	4.9
Tm	7.9	8.0	8.1	8.0	2.335	2.328	2.358	2.33	6.1	5.8
Yb	7.7	8.3		7.9	2.319	2.322		2.329	5.9	6.8
Lu	7.9	7.9	8.0		2.313	2.310	2.338		5.7	4.7

Note: Data of EXAFS, XD, and ND are listed in Appendix 1<sup>1</sup>.

Table 3 shows that the structural parameters determined in this study are almost identical to the previous data obtained using the EXAFS method. The hydration numbers are determined as 9.4–9.7 for  $\text{La}^{3+}$ - $\text{Nd}^{3+}$ , 7.5–8.1 for  $\text{Gd}^{3+}$ - $\text{Lu}^{3+}$  and 8.5–9.1 for  $\text{Sm}^{3+}$  and  $\text{Eu}^{3+}$ . The obtained values of  $\text{La}^{3+}$ ,  $\text{Ce}^{3+}$ ,  $\text{Pr}^{3+}$ , and  $\text{Nd}^{3+}$  ions are 0.2–0.8 higher than the previous data, but the rest are consistent with the compiled data, except for  $\text{Yb}^{3+}$ . The Debye-Waller factors decrease gradually from  $9.4$ – $8.7 \times 10^{-3}$  Å<sup>2</sup> for  $\text{La}^{3+}$ - $\text{Nd}^{3+}$  to  $5.5$ – $6.6 \times 10^{-3}$  Å<sup>2</sup> for  $\text{Gd}^{3+}$ - $\text{Lu}^{3+}$  through  $8.1$ – $7.1 \times 10^{-3}$  Å<sup>2</sup> for  $\text{Sm}^{3+}$ - $\text{Eu}^{3+}$ , similarly to the hydration numbers. The decreasing trend in the Debye-Waller factors is mainly the result of static disorder because the Debye-Waller factors attributable to thermal vibration change little across the REE series (Yamaguchi et al. 1988). The interatomic distances also decrease from 2.55 to 2.31 Å from  $\text{La}^{3+}$  to  $\text{Lu}^{3+}$ . The hydration parameters of  $\text{Sm}^{3+}$  and  $\text{Eu}^{3+}$  are always intermediate between those of the light REEs ( $\text{La}^{3+}$ - $\text{Nd}^{3+}$ ) and those of the heavy REEs ( $\text{Gd}^{3+}$ - $\text{Lu}^{3+}$ ). Habenschuss and Spedding (1980) suggested that the middle of the REE series is the intermediate sphere. Kanno and Hiraishi (1980) and Kowall et al. (1995) supported the conjecture that  $\text{Sm}^{3+}$ ,  $\text{Eu}^{3+}$ , and  $\text{Gd}^{3+}$  exist in two different coordination spheres based on the data of Raman spectroscopy and molecular dynamic simulation. That problem is discussed in the following section.

Actually,  $\text{Y}^{3+}$  has a similar ionic radius to  $\text{Ho}^{3+}$ ; consequently, both hydration structures are similar. Table 2 shows that the determined structure parameters of  $\text{Y}^{3+}$  are almost identical to those of  $\text{Ho}^{3+}$  within errors, except for the shift of  $E_0$ . The determined interatomic distance (2.36 Å) and the Debye-Waller factor ( $6.4 \times 10^{-3}$  Å<sup>2</sup>) of  $\text{Y}^{3+}$  ion are consistent with the previous data (2.36 Å and  $6.1 \times 10^{-3}$  Å<sup>2</sup>), but the hydration number (7.5) is much smaller than the previous EXAFS value (9.0) in Table 3. The analogy between hydration states of  $\text{Y}^{3+}$  to  $\text{Ho}^{3+}$  ions in Table 2 suggests that the  $\text{Y}^{3+}$  ion has an octahydrated structure in solution (Lindqvist-Reis et al. 2000).

### Change of hydration numbers of $\text{REE}^{3+}$ ions

The hydration numbers obtained using the EXAFS measurements of  $\text{REE}^{3+}$  ions in 1 M  $\text{HNO}_3$  solutions are shown in Figure 6. The determined hydration numbers change as a sigmoid curve from about 9.6 for  $\text{La}^{3+}$ - $\text{Nd}^{3+}$  and about 7.9 for  $\text{Gd}^{3+}$ - $\text{Lu}^{3+}$ . A

considerable discontinuity in hydration numbers is depicted in Figure 6. The hydration numbers of  $\text{Sm}^{3+}$  and  $\text{Eu}^{3+}$  are plotted between the two regions. It is difficult to conclude that the hydration numbers of  $\text{Sm}^{3+}$  and  $\text{Eu}^{3+}$  ions are in a transitional zone between eight and nine because of their large errors. Therefore, the hydration states of  $\text{REE}^{3+}$  ions are characterized using interatomic distances because these parameters are determined more accurately than the hydration numbers.

Figure 7 shows the interatomic distances of  $\text{REE}^{3+}$ - $\text{OH}_2$ . The errors are smaller than the symbols. The ionic radii of cation and anion are known to become larger with increasing coordination number (e.g., Shannon and Prewitt 1969). For comparison, the mean REE-O distances are estimated from various REE complexes with coordination numbers (CN) of eight and nine (see Appendix 2) and are plotted in Figure 7. Appendix 2 Table 1<sup>1</sup> shows data of hydrated REE complexes consisting of the eight-coordination and nine-coordination spheres (Gerkin and Reppart 1984; Ohki et al. 1988; Harrowfield et al. 1994; Junk et al. 1999a, 1999b, 1999c; Lim et al. 2000). Marcus (1988) suggested that the ionic radii obtained from the mean ion-water distances are comparable to the Pauling-type crystal ionic radii. Therefore, the interatomic distances of hydrated  $\text{REE}^{3+}$  ions can be compared directly with those of REE compounds. Figure 7 shows that interatomic distances of aqueous light  $\text{REE}^{3+}$  (from  $\text{La}^{3+}$  to  $\text{Nd}^{3+}$ ) ions are plotted on or near the line of REE-O data with CN = 9; those of aqueous heavy  $\text{REE}^{3+}$  (from  $\text{Tb}^{3+}$  to  $\text{Lu}^{3+}$ ) ions are plotted on or near the REE-O data with CN = 8. The interatomic distances of aqueous  $\text{Sm}^{3+}$ ,  $\text{Eu}^{3+}$ , and  $\text{Gd}^{3+}$  ions are plotted in the middle of REE-O data with CN = 8 and CN = 9. It is concluded precisely that light REEs ( $\text{La}^{3+}$ - $\text{Nd}^{3+}$ ) have a nonhydrated structure, heavy REEs ( $\text{Tb}^{3+}$ - $\text{Lu}^{3+}$ ) have an octahydrated structure, and  $\text{Sm}^{3+}$ ,  $\text{Eu}^{3+}$ , and  $\text{Gd}^{3+}$  are transitional between nonhydrated and octahydrated structures or a mixture of two hydrated structures.

### Relationship between hydration change of $\text{REE}^{3+}_{(\text{aq})}$ and thermodynamic quantities

Now we know where the hydration change occurs based on the results of EXAFS analysis. The geochemical importance of the hydration change of  $\text{REE}^{3+}_{(\text{aq})}$  on REE(III) reactions has been thoroughly discussed by Kawabe (1999a, 1999b) and Kawabe

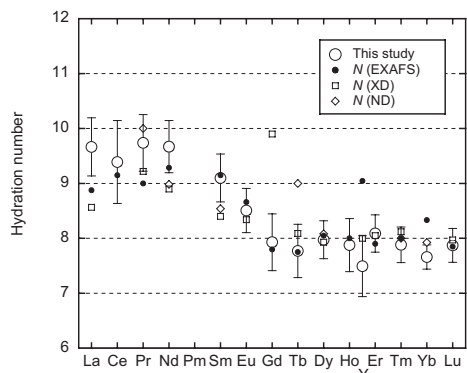


FIGURE 6. Hydration numbers of REE<sup>3+</sup> ions determined in this study and reference data obtained using the XD, ND, and EXAFS methods.

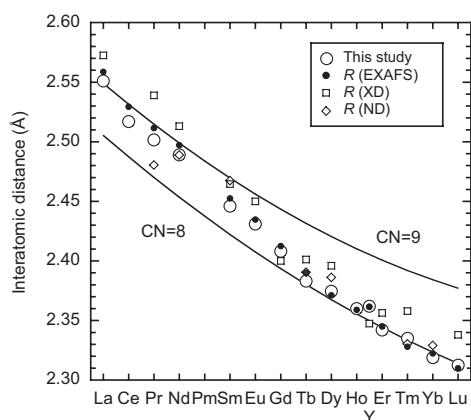


FIGURE 7. Interatomic distances of REE<sup>3+</sup>-OH<sub>2</sub> determined in this study and the reference data. Solid lines (CN = 8 and 9) indicate the mean REE-O distances obtained from REE complexes consisting of the eight-coordination and nine-coordination spheres (see Appendix 2).

et al. (2006a, 2006b). According to their suggestion, we show the effect of hydration change on geochemical reactions and the relationships between interatomic distances and thermodynamic parameters. Kawabe (1999b) and Kawabe et al. (1999) reported that the series variations of REE complex formation reactions with carbonate ions and of REE partitioning between Fe hydroxide and solution show the depletion in light REEs. They pointed out that the irregularity is due to the hydration change in REE<sup>3+</sup> series. Miyakawa et al. (1988) and Kawabe (1999a) independently estimated thermodynamic parameters for the hydration change in the REE<sup>3+</sup> series. They concluded that nonahydrated REE<sup>3+</sup> [REE(H<sub>2</sub>O)<sub>9</sub><sup>3+</sup>] is more stable than octahydrated REE<sup>3+</sup> [REE(H<sub>2</sub>O)<sub>8</sub><sup>3+</sup>] for light REE<sup>3+</sup>. Kawabe (1999a) suggested that the difference of the hydration enthalpy between real REE<sup>3+</sup> [a mixture of REE(H<sub>2</sub>O)<sub>9</sub><sup>3+</sup> and REE(H<sub>2</sub>O)<sub>8</sub><sup>3+</sup>] and REE(H<sub>2</sub>O)<sub>8</sub><sup>3+</sup> decreased gradually from -16.9 kJ/mol in La<sup>3+</sup> to -0.06 kJ/mol in Gd<sup>3+</sup>.

The hydration enthalpy ( $-\Delta H_{\text{hyd}}^0$ ) and lattice energy ( $U$ ) of REE(III) complexes are empirically given by a linear function of the reciprocal of interatomic distances ( $R$ ) as follows (e.g., Bratsch and Silber 1982; Kawabe et al. 2006b):

$$-\Delta H_{\text{hyd}}^0 \text{ or } U = A/R + B \quad (5)$$

where  $A$  and  $B$  are constants. Equation 5 indicates that determining the coordination states of REE<sup>3+</sup> ions in solution (and also in solid phases) relates indirectly to estimation of bonding energy for REE(III) complexes. Kawabe et al. (2006b) further emphasized that the empirical linear relationship between  $-\Delta H_{\text{hyd}}^0$  and the reciprocal of REE-OH<sub>2</sub> distance includes not only electrostatic energy but also a quantum mechanism (the tetrad effect or the nephelauxetic effect). Therefore, determining the structures of REE<sup>3+</sup> (and other REE<sup>3+</sup> complexes) subserves thermodynamic and theoretical elucidation of various REE(III) reactions between solid and liquid phases.

## ACKNOWLEDGMENTS

The EXAFS experiments were performed under the approval of the Photon Factory Program Advisory Committee (2001G122, 2002G257, 2004G321, and 2005G228). The authors are grateful to Tomoko Handa, Akiko Naitoh, Tetsuaki Yoshida, Satoshi Fukura, Tazuko Morimoto, and Shoko Odake for their help in measuring the EXAFS spectra at KEK-PF. The authors also thank Noboru Imai, Shigeru Terashima, Takashi Okai, Masumi Mikoshiba (Ujiie), Shigeo Togashi, and Ran Kubota for their valuable discussions.

## REFERENCES CITED

- Allen, P.G., Bucher, J.J., Shuh, D.K., Edelstein, N.M., and Craig, I. (2000) Coordination chemistry of trivalent lanthanide and actinide ions in dilute and concentrated chloride solutions. *Inorganic Chemistry*, 39, 595–601.
- Anderson, A.J., Jayanetti, S., Mayanovic, R.A., Bassett, W.A., and Chou, I-M. (2002) X-ray spectroscopic investigations of fluids in the hydrothermal diamond anvil cell: The hydration structure of aqueous La<sup>3+</sup> up to 300 °C and 1600 bars. *American Mineralogist*, 87, 262–268.
- Ankudinov, A.L., Bouldin, C.E., Rehr, J.J., Sims, J., and Hung, H. (2002) Parallel calculation of electron multiple scattering using Lanczos algorithms. *Physical Review B: Condensed Matter and Materials Physics*, 65, 104107.1–104107.11.
- Annis, B.K., Hahn, R.L., and Narten, A.H. (1985) Hydration of the Dy<sup>3+</sup> ion in dysprosium chloride solutions determined by neutron diffraction. *The Journal of Chemical Physics*, 82, 2086–2091.
- Beall, G.W., Milligan, W.O., and Wolcott, H.A. (1977) Structure trends in the lanthanide trihydroxides. *Journal of Inorganic and Nuclear Chemistry*, 39, 65–70.
- Bénazeth, S., Purans, J., Chalbot, M.-C., Nguyen-van-Duong, M.K., Nicolas, L., Keller, F., and Gaudemer, A. (1998) Temperature and pH dependence XAFS study of Gd(DOTA)<sup>-</sup> and Gd(DTPA)<sup>2-</sup> complexes: Solid state and solution structures. *Inorganic Chemistry*, 37, 3667–3674.
- Bratsch, S. and Silber, H.B. (1982) Lanthanide thermodynamic predictions. *Polyhedron*, 1(3), 219–223.
- Chaboy, J. and Tyson, T. A. (1994) Relative cross sections for bound-state double-electron  $LN_{4s}$ -edge transitions. *Physical Review*, B49, 5869–5875.
- Chaboy, J., Marcelli, A., and Tyson, T. A. (1994) Influence of double-electron transitions on the EXAFS  $L$  edges of rare-earth systems. *Physical Review*, B49, 11652–11661.
- Choppin, G.R. and Bertha, S.L. (1973) Lanthanide complexation: Inner vs. outer sphere. *Journal of Inorganic and Nuclear Chemistry*, 35, 1309–1312.
- Choppin, G.R., Henrie, D.E., and Buijs, K. (1966) Environmental effects on f-f transitions. I. Neodymium(III). *Inorganic Chemistry*, 5, 1743–1748.
- Cossy, C., Barnes, A.C., Enderby, J.E., and Merbach, A.E. (1989) The hydration of Dy<sup>3+</sup> and Yb<sup>3+</sup> in aqueous solution: A neutron scattering first order difference study. *The Journal of Chemical Physics*, 90, 3254–3260.
- D'Angelo, P., Pavel, N.V., and Borowski, M. (2001)  $K$ - and  $L$ -edge XAFS determination of the local structure of aqueous Nd(III) and Eu(III). *Journal of Synchrotron Radiation*, 8, 666–668.
- Filippini, A., Bernieri, E., and Mobilio, S. (1988) The multielectron excitations in X-ray-absorption spectra of a-Si:H. *Physical Review B: Condensed Matter*, 38, 3298–3304.
- Gerkin, R.E. and Reppart, W.J. (1984) The structures of the lanthanide ethyl sulfate enneahydrates,  $M(\text{C}_2\text{H}_5\text{SO}_4)_3 \cdot 9\text{H}_2\text{O}$  [ $M = \text{La-Lu}$  (except Pm)], at 171 K. *Acta Crystallographica*, C40, 781–786.
- Habenschuss, A. and Spedding, F.H. (1979a) The coordination (hydration) of rare-earth ions in aqueous chloride solutions from X-ray diffraction. I. TbCl<sub>3</sub>, DyCl<sub>3</sub>, ErCl<sub>3</sub>, TmCl<sub>3</sub>, and LuCl<sub>3</sub>. *The Journal of Chemical Physics*, 70, 2797–2806.
- (1979b) The coordination (hydration) of rare-earth ions in aqueous chloride solutions from X-ray diffraction. II. LaCl<sub>3</sub>, PrCl<sub>3</sub>, and NdCl<sub>3</sub>. *The Journal of Chemical Physics*, 70, 3758–3763.
- (1980) The coordination (hydration) of rare-earth ions in aqueous chloride solutions from X-ray diffraction. III. SmCl<sub>3</sub>, EuCl<sub>3</sub>, and series behavior. *The Journal of Chemical Physics*, 73, 442–450.

- Harrowfield, J.M., Weimin, L., Skelton, B.W., and White, A.H. (1994) Structural systematics of rare earth complexes. I Structural characterization of lanthanoid(III) picrate hydrates: Monoclinic ( $P2_1/c$ ) (quasi-)dodecahydrates of the related La  $\rightarrow$  Pr and Nd  $\rightarrow$  Tb families. *Australian Journal of Chemistry*, 47, 321–337.
- Helm, L. and Merbach, A.E. (1991) Structure and dynamics of lanthanide(III) ions in solution: a neutron scattering contribution. *European Journal of Solid State and Inorganic Chemistry*, 28, 245–250.
- Ishiguro, S., Umebayashi, Y., Kato, K., Takahashi, R., and Ozutsumi, K. (1998) Strong and weak solvation steric effects on lanthanoid(III) ions in N,N-dimethylformamide–N,N-dimethylacetamide mixtures. *Journal of the Chemical Society: Faraday Transactions*, 94, 3607–3612.
- Johansson, G. and Wakita, H. (1985) X-ray investigation of the coordination and complex formation of lanthanoid ions in aqueous perchlorate and selenate solutions. *Inorganic Chemistry*, 24, 3047–3052.
- Johansson, G. and Yokoyama, H. (1990) Inner- and outer-sphere complex formation in aqueous erbium halide and perchlorate solutions. An X-ray diffraction study using isostructural substitution. *Inorganic Chemistry*, 29, 2460–2466.
- Johansson, G., Niinistö, L., and Wakita, H. (1985) Coordination of the trivalent lanthanoids in aqueous selenate and perchlorate solutions. *Acta Chemica Scandinavica*, A39, 359–361.
- Junk, P.C., Kepert, C.J., Wei-Min, L., Skelton, B.W., and White, A.H. (1999a) Structural systematics of rare earth complexes. XI (maximally) Hydrated rare earth(III) trifluoro- and trichloro-acetates. *Australian Journal of Chemistry*, 52, 459–479.
- Junk, P.C., Kepert, C.J., Skelton, B.W., and White, A.H. (1999b) Structural systematics of rare earth complexes. XX (maximally) Hydrated rare earth sulfates and the double sulfates  $(\text{NH}_4)_2\text{Ln}(\text{SO}_4)_2 \cdot 4\text{H}_2\text{O}$  (Ln = La, Tb). *Australian Journal of Chemistry*, 52, 601–615.
- Junk, P.C., Kepert, C.J., Wei-Min, L., Skelton, B.W., and White, A.H. (1999c) Structural systematics of rare earth complexes. X (maximally) Hydrated rare earth acetates. *Australian Journal of Chemistry*, 52, 437–457.
- Kanno, J. and Hiraishi, J. (1980) Raman spectroscopic evidence for a discrete change in coordination number of rare earth aquo-ions in the middle of the series. *Chemical Physics Letters*, 75, 553–556.
- Kawabe, I. (1999a) Thermochemical parameters for solution of lanthanide(III) ethylsulphate and trichloro hydrate series: Tetrad effects and hydration change in aqua  $\text{Ln}^{3+}$  ion series. *Geochemical Journal*, 33, 249–265.
- (1999b) Hydration change of aqueous lanthanide ions and tetrad effects in lanthanide(III)-carbonate complexation. *Geochemical Journal*, 33, 267–275.
- Kawabe, I., Ohta, A., Ishii, S., Tokumura, M., and Miyauchi, K. (1999) REE partitioning between Fe-Mn oxyhydroxide precipitates and weakly acid NaCl solutions: Convex tetrad effect and fractionation of Y and Sc from heavy lanthanides. *Geochemical Journal*, 33, 167–179.
- Kawabe, I., Takahashi, T., Tanaka, K., and Ohta, A. (2006a) Hydration change reaction of light REE $_{\text{aq}}^{3+}$  series-I: An important constraint on REE(III) partitioning and complex formation reactions in low-temperature to hydrothermal condition. *The Journal of Earth and Planetary Sciences*, Nagoya University, 53, 33–50.
- (2006b) Hydration change reaction of light REE $_{\text{aq}}^{3+}$  series-II: Contrasting nephelauxetic effects between hydrated  $[\text{REE}(\text{H}_2\text{O})_9]^{3+}$  and  $[\text{REE}(\text{H}_2\text{O})_8]^{3+}$  series and the tetrad effects in their hydration enthalpies and REE–OH $_2$  distances. *The Journal of Earth and Planetary Sciences*, Nagoya University, 53, 51–71.
- Kodre, A., Arçon, I., Hribar, M., Štuehec, M., Villain, F., and Parent P. (1994) Double photoexcitation  $[2(s,p)4(p,d)]$  in the Xe-isoelectronic series  $\text{Cs}^+$ ,  $\text{Ba}^{2+}$ ,  $\text{La}^{3+}$ . *Journal de Physique. Colloque*, C9, 397–400.
- Kowall, Th., Foglia, F., Helm, L., and Merbach, A.E. (1995) Molecular dynamics simulation study of lanthanide ions  $\text{Ln}^{3+}$  in aqueous solution including water polarization. Change in coordination number from 9 to 8 along the series. *Journal of the American Chemical Society*, 117, 3790–3799.
- Lim, K.C., Skelton, B.W., and White, A.H. (2000) Structural systematics of rare earth complexes. XXII (maximally) hydrated rare earth iodides. *Australian Journal of Chemistry*, 53, 867–873.
- Lindqvist-Reis, P., Lamble, K., Pattanaik, S., Persson, I., and Sandström, M. (2000) Hydration of the yttrium(III) ion in aqueous solution. An X-ray diffraction and XAFS structural study. *Journal of Physical Chemistry*, B104, 402–408.
- Marcus, Y. (1988) Ionic radii in aqueous solutions. *Chemical Reviews*, 88, 1475–1498.
- Mayanovic, R.A., Jayanetti, S., Anderson, A.J., Bassett, W.A., and Chou, I.-M. (2002) The structure of  $\text{Yb}^{3+}$  aquo ion and chloro complexes in aqueous solutions at up to 500 °C and 270 MPa. *Journal of Physical Chemistry*, A106, 6591–6599.
- Miyakawa, K., Kaizu, Y., and Kobayashi, H. (1988) An electrostatic approach to the structure of hydrated lanthanoid ions.  $[\text{M}(\text{OH}_2)_9]^{3+}$  versus  $[\text{M}(\text{OH}_2)_8]^{3+}$ . *Journal of the Chemical Society: Faraday Transactions I*, 84, 1517–1529.
- Narten, A.H. and Hahn, R.L. (1982) Direct determination of ionic solvation from neutron diffraction. *Science*, 217, 1249–1250.
- (1983) Hydration of the  $\text{Nd}^{3+}$  ion in neodymium chloride solutions determined by neutron diffraction. *Journal of Physical Chemistry*, 87, 3193–3197.
- Näslund, J., Lindqvist-Reis, P., Persson, I., and Sandström, M. (2000) Steric effects control the structure of the solvated lanthanum(III) ion in aqueous, dimethyl sulfoxide, and N,N'-dimethylpropyleneurea solution. An EXAFS and large-angle X-ray scattering study. *Inorganic Chemistry*, 39, 4006–4011.
- Nomura, M. (1998) Dead-time correction of a multi-element SSD for fluorescent XAFS. *Journal of Synchrotron Radiation*, 5, 851–853.
- Nomura, M. and Koyama, A. (1996) Design and performance of a new XAFS beamline at the Photon Factory; BL-12C. KEK Report, 95-15, 1–21.
- Ohki, Y., Suzuki, Y., Takeuchi, T., and Ouchi, A. (1988) The crystal and molecular structure of scandium(III), yttrium(III), and some lanthanoid(III) p-toluenesulfonates,  $[\text{Sc}(\text{C}_7\text{H}_7\text{SO}_3)_2(\text{H}_2\text{O})_6][\text{C}_7\text{H}_7\text{SO}_3] \cdot 2\text{H}_2\text{O}$  and  $[\text{M}(\text{C}_7\text{H}_7\text{SO}_3)_2(\text{H}_2\text{O})_6][\text{C}_7\text{H}_7\text{SO}_3] \cdot 3\text{H}_2\text{O}$  (M=Y, Sm, Gd, Dy, Ho, Er, Yb); and yttrium(III) and dysprosium(III) 2-naphthalenesulfonates,  $[\text{M}(\text{C}_{10}\text{H}_7\text{SO}_3)_2(\text{H}_2\text{O})_6][\text{C}_{10}\text{H}_7\text{SO}_3] \cdot 3\text{H}_2\text{O}$  (M=Y, Dy). *Bulletin of the Chemical Society of Japan*, 61, 393–405.
- Ohta, A. and Kawabe, I. (2001) REE adsorption onto Mn dioxide ( $\delta\text{-MnO}_2$ ) and Fe oxyhydroxide: Ce(III) oxidation by  $\delta\text{-MnO}_2$ . *Geochimica et Cosmochimica Acta*, 65, 695–703.
- Ohtaki, H. and Radnai, T. (1993) Structure and dynamics of hydrated ions. *Chemical Reviews*, 93, 1157–1204.
- Ragnarsdottir, K.V., Oelkers, E.H., Sherman, D.M., and Collins, C.R. (1998) Aqueous speciation of yttrium at temperatures from 25 to 340 °C at  $p_{\text{sat}}$ : an in situ EXAFS study. *Chemical Geology*, 151, 29–39.
- Rizkalla, E.N. and Choppin, G.R. (1991) Hydration and hydrolysis of lanthanides. In K.A. Gschneidner, Jr. and L. Eyring, Eds., *Handbook on the Physics and Chemistry of Rare Earths*, 15, p. 393–442. Elsevier Science B.V., Amsterdam.
- Russ, A.I., Lesovitskaya, M.K., and Shapovalov, I.M. (1978) X-ray diffraction study of aqueous solutions of samarium and gadolinium chlorides. *Chemical Abstracts*, 89, 95116.
- Shannon, R.D. and Prewitt, C.T. (1969) Effective ionic radii in oxides and fluorides. *Acta Crystallographica*, B25, 925–946.
- Solera, J.A., García, J., and Proietti, M.G. (1995) The multielectron excitations at the L edges in rare-earth ionic aqueous solutions. *Physical Review*, B51, 2678–2686.
- Yamaguchi, T., Nomura, M., Wakita, H., and Ohtaki, H. (1988) An extended X-ray absorption fine structure study of aqueous rare earth perchlorate solutions in liquid and glassy states. *The Journal of Chemical Physics*, 89, 5153–5159.
- Yamaguchi, T., Tanaka, S., Wakita, H., Misawa, M., Okada, I., Soper, A.K., and Howells, W.S. (1991) Pulsed neutron diffraction studies on lanthanide(III) hydration in aqueous perchlorate solutions. *Zeitschrift für Naturforschung*, 46a, 84–88.

MANUSCRIPT RECEIVED MARCH 1, 2007

MANUSCRIPT ACCEPTED JANUARY 21, 2008

MANUSCRIPT HANDLED BY ANDREAS LUTTGE

## APPENDIX 2

The ionic radii of cations and anions become larger with increasing coordination number (e.g., Shannon and Prewitt 1969); that is, the REE–O distance changes systematically according to the size of the first coordination sphere. The empirical interatomic distances are estimated using hydrated REE complexes whose first coordination sphere is occupied only by oxygen. Appendix 2 Table 1<sup>1</sup> shows data of hydrated REE complexes consisting of the eight-coordination and nine-coordination spheres. Appendix 2 Figure 1<sup>1</sup> shows that the data are fitted by the curve of the second order to determine the mean interatomic distances (R); the following results were obtained:

$$R_{(\text{CN}=8)} = 3.288 \times 10^{-4}(Z-56)^2 - 1.893 \times 10^{-2}(Z-56) + 2.524, \quad (\text{A1})$$

and

$$R_{(\text{CN}=9)} = 4.011 \times 10^{-4}(Z-56)^2 - 1.869 \times 10^{-2}(Z-56) + 2.567 \quad (\text{A2})$$

where Z indicates the atomic number. The mean interatomic distances calculated by Equations 1 and 2 are shown in Appendix 2 Table 2<sup>1</sup>.